Enhanced interfacial toughness of thermoplastic-epoxy interfaces using ALD surface treatments

Yuxin Chen[1], Nicholas J. Ginga[1], William S. LePage[1], Eric Kazyak[1], Andrew J. Gayle[1], Jing Wang[1], Robin E. Rodríguez[1], M. D. Thouless[1,2], Neil P. Dasgupta[1,*]

[1]*Department of Mechanical Engineering, University of Michigan, Ann Arbor, MI 48109, USA*

[2]*Department of Materials Science and Engineering, University of Michigan, Ann Arbor, MI 48109, USA*

ABSTRACT

Interfacial fracture and delamination of polymer interfaces can play a critical role in a wide range of applications, including fiber-reinforced composites, flexible electronics, and encapsulation layers for photovoltaics. However, owing to the low surface energy of many thermoplastics, adhesion to dissimilar material surfaces remains a critical challenge. In this work, we demonstrate that surface treatments using atomic layer deposition (ALD) on poly (methyl methacrylate) (PMMA) and fluorinated ethylene propylene (FEP) lead to significant increases in surface energy, without affecting the bulk mechanical response of the thermoplastic. After ALD film growth, the interfacial toughness of the PMMA-epoxy and FEP-epoxy interfaces increased by up to factor of 7 and 60, respectively. These results demonstrate the ability of ALD to engineer the adhesive properties of chemically inert surfaces. However, in the present case, the interfacial toughness was observed to decrease significantly with an increase in humidity. This was attributed to the phenomenon of stress-corrosion cracking associated with the reaction between Al_2O_3 and water, and may have a significant implication for the design of these tailored interfaces.

[*]Correspondence to: ndasgupt@umich.edu

KEYWORDS Adhesion, Interfacial Toughness, Atomic-Layer Deposition, Vapor-Phase Infiltration, Polymers

INTRODUCTION

Thermoplastics, such as poly(methyl methacrylate) (PMMA) and fluorinated ethylene propylene (FEP), have widespread applications in consumer products, structural components, biomedical devices[1], and electronics[2]. In many of these applications, formation of an adhesive bond between the thermoplastic and a dissimilar material surface is crucial. For example, in aerospace and space applications, thermoplastic-epoxy interfaces play a critical rule in toughening the bulk composite.[3] However, for an adhesive to wet and bond effectively to a surface, the surface energy of the substrate must be equal to or higher than the surface energy of the adhesive [4]. Common thermoplastics have surface energies of ~20-45 mJ m^{-2} [5], which are lower than the surface energies of polymeric adhesives, such as epoxies (~45-50 mJ m^{-2}) [6]. Therefore, in order to improve adhesion, there is a need for new methods to increase the surface energy of thermoplastics without changing their bulk properties.

Several pre-treatment methods have been developed to increase the surface energy of polymers. For example, nano-fabrication techniques have been used to introduce surface structuring[7]. Chemical treatments have also been explored, including soaking the polymer in a solution of reactive molecules[8], exposing the surface to solvents[9], and grafting the surface with a monomer[10]. Plasma treatments have also been applied to a variety of polymers, including polydimethylsiloxane (PDMS), Kapton, and polypropylene[11–13]. Plasma treatment of PMMA has been shown to introduce cross-linking on a subsurface layer of 150 nm or thicker, thus

increasing its surface energy[14,15]. Flame treatment can also enhance adhesion by reorienting oxygen containing functional groups near surface[16]. Additionally, mechanical treatments, including grit blasting, can be used to improve wettability of polymer surfaces[9]. However, many of these approaches lead to undesirable changes in either the bulk properties or surface roughness of the polymer, motivating the search for new methods to decouple surface chemistry from the morphology and bulk response of the underlying material.

An alternative method to increase the surface energy of polymers is atomic-layer deposition (ALD) of metal-oxide thin films[17–19]. ALD is a modified chemical vapor deposition technique based on sequential exposure of gas-phase reactants that exhibit self-limiting surface reactions. Ideal ALD processes deposit films in a layer-by-layer fashion, providing sub-nanometer control of film thickness[20]. ALD is also known for creating conformal, pin-hole free films over large areas or high aspect ratio substrates[21]. Moreover, several ALD processes are feasible at low temperatures, allowing for ALD on low-melting-point materials such as polymers. For instance, deposition temperatures as low as 33 ºC have been reported for ALD Al_2O_3, which is below the glass transition temperature for many polymers[22].

Unlike the ideal ALD model described above, when ALD is performed on certain polymers, gas-phase reactants can diffuse into the polymer, causing subsurface reactions and entrapment within the polymer chains[23,24]. This has led to the development of a range of vapor-phase polymer treatments that fall within the category of vapor phase infiltration (VPI)[23,25,26]. In VPI

processes, the subsurface region forms an interphase that is often composed of a hybrid between the organic substrate and the inorganic ALD film. Since VPI processes depend on several concurrent processes, including diffusion, adsorption, and chemical reactions, they are highly dependent on the selection of both the polymer and ALD precursor, and can be influenced by temperature and exposure time[23,27–29].

In this work, we demonstrate that ALD surface treatments can be applied on PMMA and FEP to increase interfacial toughness when bonded to an epoxy, which corresponds with an increase in surface energy. Cross-sectional transmission electron microscopy (TEM) and atomic force microscopy (AFM) were used to characterize the film morphology, and sessile drop tests were used to measure the surface energies before and after ALD. The interfacial toughness of the polymer-epoxy interfaces was measured in the double-cantilever-beam (DCB) geometry. After ALD surface treatment, the interfacial toughness of the PMMA-epoxy interface increased by 7 times and the interfacial toughness of the FEP-epoxy interface increased by 60 times in a dry environment. Furthermore, as ambient humidity increased, the interfacial toughness decreased, which is a common characteristic of adhesive interfaces on metal oxides.

EXPERIMENTAL SECTION

Atomic-Layer Deposition (ALD)

Polymer substrates were cut from extruded sheets of PMMA (Acrylite® FF), and FEP (Teflon® FEP 100). Before any treatment, the PMMA and FEP samples were thoroughly cleaned by sonication in water and rinsing in solvents (further details in SI). ALD was performed in a Savannah S200 (Veeco/Cambridge Nanotech Inc.). Trimethylaluminum (TMA) and water were evaporated at room temperature as the precursors. The carrier gas was ultrahigh purity argon flowing at 10 sccm. During film growth, each precursor was pulsed into the chamber for t_1, then the chamber was closed for t_2 to allow the precursor to diffuse onto and partially into the substrate, and finally the chamber was purged with argon for t_3 to remove the excess precursor. For the TMA half cycles, t_1, t_2, and t_3 were 0.1 s, 10 s and 45 s, respectively. For the water half cycles, t_1, t_2, and t_3 were 0.02 s, 10 s and 45 s, respectively. During the holds, carrier gas was constantly flowing at 5 sccm, as we do not have a valve to isolate the MFC from the chamber. Therefore, the total pressure constantly rose in the range of 1-5 torr during the exposure. The substrate temperature was maintained at 65 ºC for PMMA samples, and 74 ºC for FEP samples. 750 cycles of were performed for both polymers.

Materials Characterization

AFM measurements were performed using a Veeco Dimension® Icon™ atomic-force microscope. Cross-sectional, transmission-electron-mircoscopy (TEM) analysis was performed

using a JEOL 2100 probe-corrected analytical electron microscope after a lift-out procedure with a focused ion beam (FIB). Spectroscopic ellipsometry was conducted with a Woollam M-2000. A Kratos Axis Ultra with a monochromated Al source was used for X-ray photoelectron-spectroscopy (XPS) analysis. Scanning-electron microscopy (SEM) with energy-dispersive x-ray spectroscopy (EDS) was performed inside a TESCAN MIRA3 FEG-SEM.

Sessile-Drop Test

Sessile-drop tests on as-received, cleaned, vacuum-annealed, and ALD-treated samples were conducted to measure the surface energies. Contact angles were measured between the polymers and water, glycerol, hexadecane, ethylene glycol and octane. All contact-angle measurements are provided in Tables S1 and S2. Surface energies were calculated using relationships derived by Oss *et al*.[30], and liquid surface energies were used from Preston *et al*.[31] (further details in SI).

Fabrication of Double-Cantilever-Beam Samples

The double-cantilever-beam (DCB) samples consisted of two identical polymer beams bonded by an epoxy layer (Figure 1a). Each beam was 25.4 mm wide, 76.2 mm long, and 2.38 mm thick. Before applying the epoxy, a 30 nm thick gold film was deposited onto one of the beams using e-beam evaporation through a shadow mask. The purpose of this film was to form a pre-crack at a known interface with a defined length of 25 mm. For ALD-coated samples, the pre-crack was

deposited after ALD. The adhesive was a two-component epoxy (EPO-TEK 353-ND). To control the thickness of the epoxy layer, 23-26 μm soda-lime glass beads (Cospheric) were mixed into the epoxy (further details in SI). The DCB sample was clamped and cured at 60 °C for 2 hr, then at 80 °C for 35 min. The four sides of the cured samples were polished with 320, 600 and 1200 grit silica papers to remove any epoxy overflow.

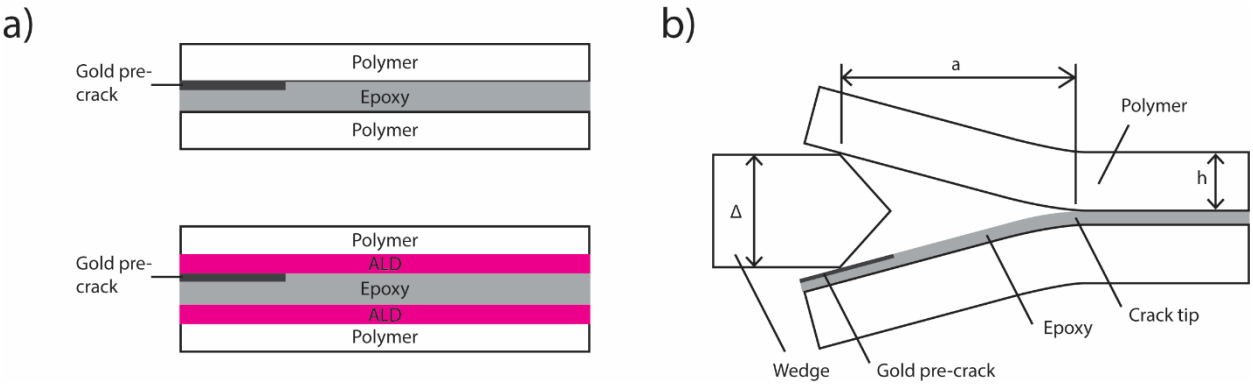

Figure 1: a) Schematic illustration of DCB samples before testing, with and without ALD interlayers. b) Geometric parameters used in the wedge test, including crack length *a*, wedge thickness *Δ* and beam thickness *h*.

Measurement of the Interfacial Toughness

The interfacial toughness of the DCB samples was measured in the wedge-test configuration (Figure 1b). The wedge was a razor blade that was 230 μm thick (*Δ*). To initiate the test, the wedge was inserted along the pre-crack. The poor adhesion of the gold to the polymer allows it to delaminate from the polymer once the wedge was inserted. The wedge was controlled by a stepper motor that pushed it into the DCB at 2 mm s^{-1}, for a total travel-length of 4 mm. Top-down digital photographs were captured periodically, beginning within 2 seconds after the wedge insertion. From each image, the area of the crack was measured, and the crack length

was defined as the crack area divided by the width of the sample (Figure S1). The time stamp for each image was used to calculate the crack speed. The test was conducted with a constant crack-mouth opening-displacement (Δ), so the energy-release rate, $\mathcal{G}$, decreased as the crack propagated.

As shown in Figure 1b, h is defined as the thickness of the polymer beam, a is the length of the crack from the contact point of the DCB with the wedge to the crack tip between the polymer and epoxy, and Δ is the thickness of the wedge. The energy-release rate, $\mathcal{G}$, was calculated as

$$\mathcal{G} = \frac{\Delta^2 \bar{E}}{h\left[8\frac{a^3}{h^3}+16.2\frac{a^2}{h^2}+10.9\frac{a}{h}+3.66\right]^2}\left[12\frac{a^2}{h^2}+16.2\frac{a}{h}+5.45\right], \quad \textbf{Eq.1}$$

where $\bar{E} = E/(1-\nu^2)$ for plane strain[32]. E is the Young's modulus of the polymer beam and ν is Poisson's ratio, which were measured separately (further details in SI). To determine the interfacial toughness, Γ, $\mathcal{G}$ was plotted as a function of crack velocity (Fig. 4). Γ is reported as the energy-release rate where the crack reached equilibrium.

RESULTS

As shown by the AFM images in Figure 2a, the ALD treatments did not significantly increase the surface roughness of the polymers. The RMS roughness of PMMA before and after ALD treatment was 1.5±0.8 nm and 1.9±1.8 nm, respectively. The RMS roughness of FEP before and after ALD treatment was 18±10 nm and 19±7 nm, respectively. The surface composition of

both polymers after ALD treatment was confirmed by XPS to be Al2O3 with an O:Al ratio of 1.5 (Figure S2). We note that it has been previously reported that hydrogen content in Al2O3 films also increases at low temperatures[22]. This demonstrates the potential of ALD to modify surface chemistry without significantly affecting morphology.

ALD treatment resulted in an Al_2O_3 film on the polymer surfaces and VPI interphases between the film and bulk polymer, as shown by cross-sectional TEM analysis (Figure 2b, c). Prior works for ALD on polymers have shown that during the initial cycles, subsurface modification can occur until a dense surface layer forms[19,20,23,28,33,34]. The extent of subsurface modification can depend on a number of variables including temperature, exposure time, precursor selection and polymer chemistry.

For the PMMA sample, the interface between the ALD and polymer appeared abrupt. Cross-sectional TEM indicated that the surface layer on PMMA was 130 nm thick (Figure 2b), while the film thickness on a silicon substrate in the same ALD run was only 110 nm. Therefore, despite the abrupt appearance of the interface between the PMMA and ALD, this discrepancy suggests that subsurface modification may have occurred in the PMMA sample. This is consistent with previous observations of ALD growth of Al_2O_3 using TMA and water as precursors on PMMA, where the initial cycles experienced a larger mass uptake before steady-state ALD growth was observed[27,33]. STEM-EDS analysis further demonstrates that Al is not present deeper within the polymer, and is confined to the region shown (Figure S3). We

note that a range in the degree of VPI into PMMA using TMA as a precursor has been reported in the literature, which depends on process variables including temperature, time and pressure[23,27–29].

In contrast, the FEP sample indicates a very clear VPI interphase (Fig. 2c) between the ALD and polymer. This interphase region resembles an organic-inorganic hybrid composite. Previous work of ALD Al_2O_3 growth on polytetrafluoroethylene (PTFE) observed a similar growth mechanism where subsurface Al_2O_3 particles formed during the initial cycles before a continuous film was developed on the surface[35].

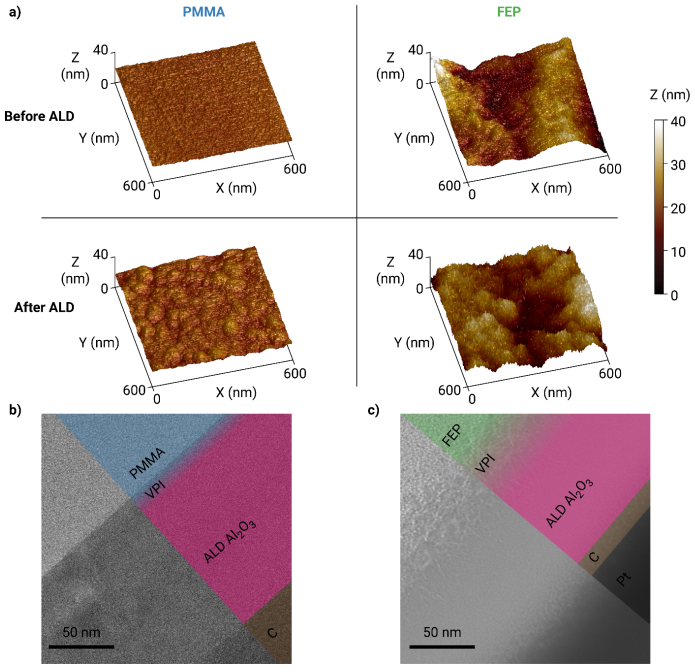

Figure 2: a) AFM scans of PMMA and FEP substrates before and after ALD surface treatment. Cross-sectional TEM analysis of b) PMMA-ALD and c) FEP-ALD samples, indicating the location of the VPI interphases. The colored regions on b) and c) are added to label each layer. These samples were treated with the same ALD procedure as the samples used for DCB fabrication.

The difference in VPI morphology on PMMA and FEP could be attributed to the distinct functional groups of the two polymers. For PMMA, the carbonyl groups on the polymer chains form covalent bonds with TMA upon exposure to the precursor[36–38]. These carbonyl reaction sites are abundant in PMMA, which could explain the more homogeneous nature of the interphase compared to FEP. In contrast, FEP has no functional groups that react with TMA. Therefore, subsurface growth relies on physical entrapment of the TMA precursor, which reacts with water in the subsequent pulse to nucleate Al_2O_3 regions within FEP[20,23].

Although ALD treatment did not significantly change the surface roughness of PMMA and FEP, it dramatically increased the surface energy of the polymers[17–19,39]. As shown in Figure 3a, ALD decreased the water contact angles for both polymers, from 70.6±1.8° to 13.4±1.0° for PMMA and from 98.4±1.0° to 15.0±0.5° for FEP. As shown in Figure 3b, the decrease in contact angles corresponds to an increase in the surface energy of PMMA from 34.5±1.0 mJ m^{-2} to 844±63 mJ m^{-2} after ALD, and an increase in the surface energy of FEP from 21.9±1.1 mJ m^{-2} to 955±224 mJ m^{-2} (calculation details in SI). These results agree with published surface energies of PMMA, FEP, and Al_2O_3, which were reported to be from 30 mJ m^{-2} to 45 mJ m^{-2} [40], from 16.9 mJ m^{-2} to 22.7 mJ m^{-2} [41], and 880 mJ m^{-2} [42], respectively. The surface energy of the polymers did not change after cleaning the samples, or after annealing the samples in vacuum under the temperature at which ALD was performed (Table S1 and S2), confirming that the change in surface energy was a result of the ALD treatment.

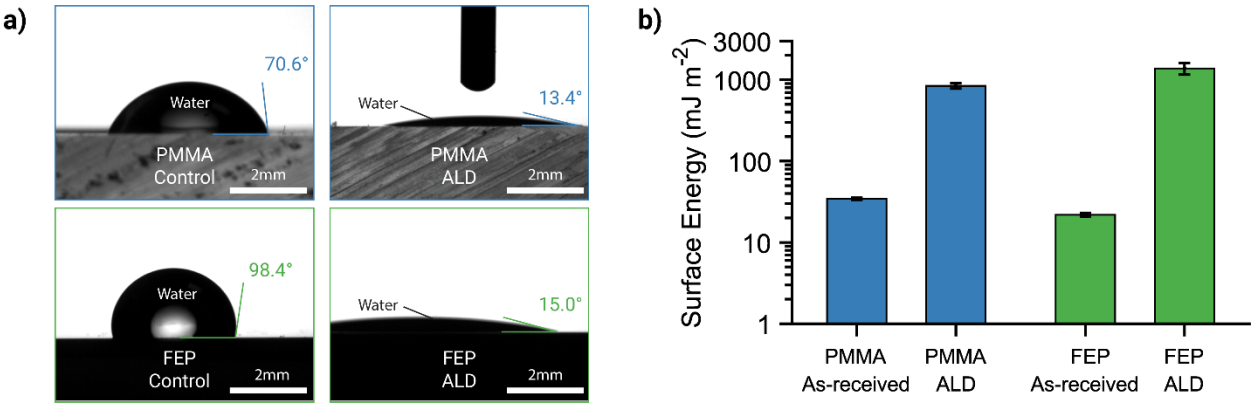

Figure 3: a) Sessile water drop tests before and after ALD treatments. b) Surface energies are calculated from contact angles with multiple liquids (further details in SI).

For a system of two materials bonded at an interface, the energy required for a crack to propagate along the interface is controlled by the interfacial toughness (Γ). Previous works have explored the ability of ALD Al_2O_3 to improve the interfacial adhesion of polymers using peel and pull-off tests[17,18].

Here, we utilize the DCB measurement technique to quantitatively probe the effect of ALD Al_2O_3 on interfacial toughness.

One of the many parameters that can influence the toughness of an interface between two materials is the work of adhesion (w_a) [43], which can be described as:

$$w_a = \gamma_1 + \gamma_2 - \gamma_{12} \qquad \textbf{Eq. 2}$$

where γ_1 and γ_2 are the surface energies of phase 1 (polymer or ALD-treated polymer) and phase 2 (epoxy), respectively, γ_{12} is the interfacial energy between phase 1 and 2[43]. Although the relationship between Γ and w_a is generally too complex to state in a simple form, often an

increase in Γ may correlate with an increase in w_a. Of particular interest for the present paper is to note that an increase in γ_1 results in an increase in w_a, and is thus expected to also be associated with an increase in interfacial toughness.

DCB measurements were performed on PMMA and FEP samples, with and without ALD treatment. After the insertion of the wedge, the crack length was observed to grow with time (Figure S4a). From the crack length at each moment in time, the energy-release rate was calculated according to Eq. 1 (Figure S4b). As the energy-release rate decreased, the crack speed also decreased, resulting in an apparent threshold for energy-release rate, below which the crack did not grow (Figure 4). This was taken to be the interfacial toughness (Γ).

After ALD treatment, the interfacial toughness of the PMMA-epoxy interface increased from 1.95±0.26 J m^{-2} to 12.6±1.4 J m^{-2}, and the interfacial toughness of FEP-epoxy interface increased from 0.25±0.03 J m^{-2} to 16.6±2.6 J m^{-2}. This represents an increase in interfacial toughness by a factor of 7 for PMMA and 60 for FEP relative to uncoated samples. Before ALD, the interfacial toughness of FEP was an order of magnitude lower than that for PMMA, which was consistent with the lower surface energy of FEP (Figure 3b). In contrast, the difference in interfacial toughness between PMMA and FEP after ALD treatment was within a factor of two, demonstrating the power of ALD to decouple surface chemistry from bulk properties. Moreover, to contextualize the observed results, the effect of an oxygen plasma pretreatment and a thinner ALD treatment with 250 ALD cycles were tested as a comparison

(see Supporting Information). To confirm that the bulk polymer response after ALD treatment did not change, tensile tests were conducted on PMMA and FEP samples with and without ALD (Figure S5).

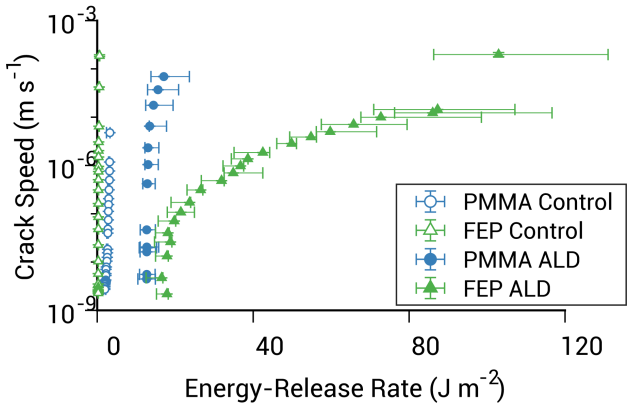

Figure 4: Crack speed vs. energy-release rate. All samples were tested at 3.5±0.5 g m^{-3} absolute humidity. Error bars in all images correspond to the variations in crack length measurement within a single image, with average values reported according to the analysis shown in Figure S1.

Interestingly, an increase in humidity generally degraded the toughness of the ALD-treated interfaces for both thermoplastics tested at 22.7±0.6 ºC (Figure 5). The fact that the toughness decreased demonstrates that the effect of humidity was to decrease the toughness of the Al_2O_3/PMMA interface, rather than simply increasing the toughness of the Al_2O_3/epoxy interface. For FEP-ALD samples, interfacial toughness decreased monotonically with humidity (Figure 5b). In contrast, for FEP-control samples, interfacial toughness remained constant at 0.32±0.06 J m^{-2} across all levels of humidity (Figure 5b). This demonstrates that the humidity dependence observed was directly caused by the ALD treatment.

For PMMA-ALD samples, the same trend of decreasing interfacial toughness with increasing humidity was observed at absolute humidity levels above 1.2±0.4 g m^{-3}. At absolute humidity level of 10.0±0.4 g m^{-3} (50±3% relative humidity at 22.7±0.6 ºC), the interfacial toughness of PMMA-ALD sample decreased to a level that is close to the PMMA control sample. For PMMA-control samples in this humidity range, interfacial toughness remained constant at 1.9±0.2 J m^{-2} (Figure 5a). The exception to this trend occurred at an absolute humidity of 0.0±0.4 g m^{-3}, where the interfacial toughness of both the PMMA-ALD and PMMA control samples decreased compared to non-zero humidity conditions (Figure 5a).

The decrease in interfacial toughness observed at zero humidity can be attributed to the plasticization effect of water on PMMA which can absorb 2.25% water at room temperature[44]. When the DCB samples were tested with the presence of water, water enhanced the plastic zone in front of the crack tip which absorbs energy as the crack propagates. This energy dissipation reduces the amount of energy available for forming new surfaces, and thus reduces the crack length at equilibrium, resulting in a higher interfacial toughness compared to PMMA in a zero humidity environment. Similar results have been observed for crack growth in PMMA[45]. Contrarily, FEP only absorbs 0.04% water even at 55 ºC[46], and thus water cannot have significant plasticization effect on it. This is consistent with the result that for FEP-control samples, no change in interfacial toughness was observed at zero humidity.

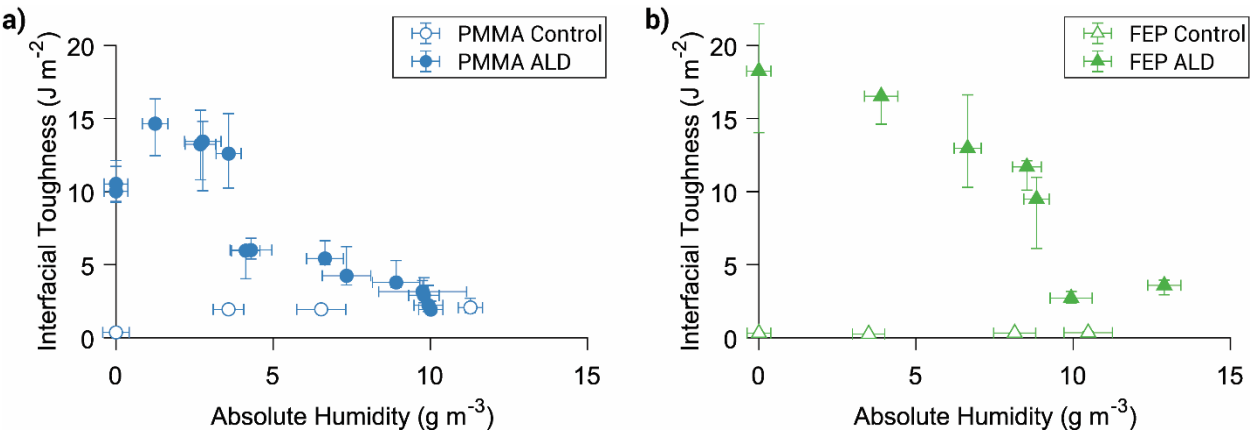

Figure 5: Humidity dependence of interfacial toughness with and without ALD treatment for a) PMMA and b) FEP. Horizontal error bars indicate the standard deviation and precision error of absolute humidity during the steady-state phase of crack growth. All experiments were performed at 22.7±0.6 ºC.

To determine the crack path, post-mortem analysis was performed using optical microscopy and SEM-EDS. An example of the edge view of a sample after wedge testing can be found in Figure S6. The crack path was further examined via SEM-EDS (Figure 6). In a dry environment (absolute humidity of 1.3±0.4 g m^{-3}), crack propagation was observed to occur along the ALD/adhesive interface (Figure 6a), demonstrating that adhesive failure occurred between the ALD and epoxy. In contrast, for the ALD-treated PMMA in a humid environment (absolute humidity of 9.9±0.5 g m^{-3}), the crack deflected along the Al_2O_3/adhesive interfaces on either side of the adhesive (Figure 6b), suggesting that the failure mechanism was affected by humidity. To demonstrate that this is reproducible, two samples tested in humid environment and two samples tested in dry environment, and the observed phenomena were consistent within each set.

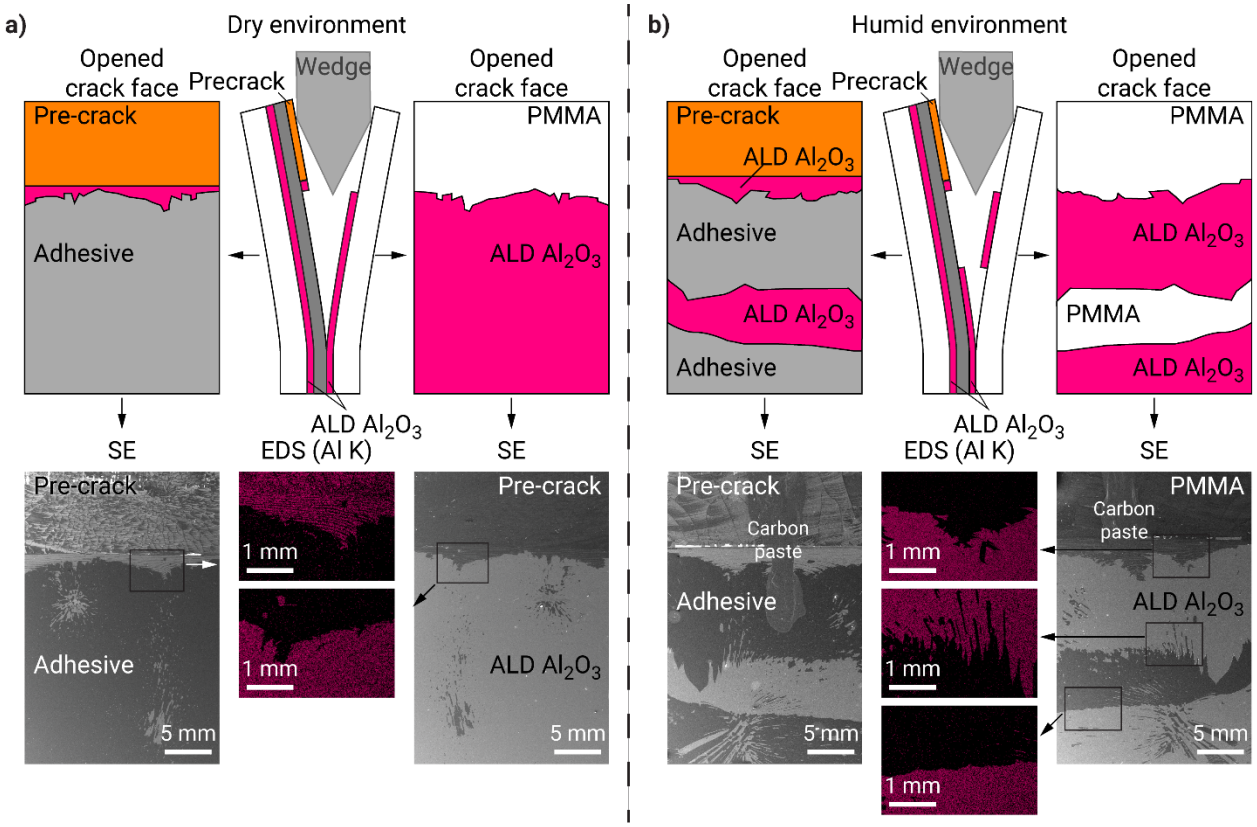

Figure 6: Post-mortem failure analysis of DCB inner-surfaces using SEM-EDS on ALD-treated PMMA that were tested at a humidity of a) 1.3±0.4 g m^{-3} and b) 9.9±0.5 g m^{-3}. Schematic representations of the failure modes are presented above the SEM images for clarity. Carbon paste was applied to the sample to reduce charging.

The fact that a strong humidity dependence on interfacial toughness was only observed in the ALD treated samples demonstrates that the observed results were not due to changes in the bulk thermoplastic or thermoplastic-epoxy interface. The humidity-dependent crack growth is consistent with the fact that Al_2O_3 is known to react with water in a stress-dependent manner, by forming hydroxide species[47]. This effect is analogous to stress-corrosion-cracking in bulk ceramics, where environmental species, such as water molecules, react with the ceramic bonds in the crack front-tip, resulting in a decrease in fracture toughness in a humid ambient[47,48]. We also note that while the interfacial toughness of ALD-treated PMMA approaches that of the

control samples at high humidity, the ALD-treated FEP interfacial toughness remains one order of magnitude larger than the uncoated control. This points towards the need to consider humidity in design applications involving ALD-modified interfaces. For example, for the encapsulation of electronic devices, including solar cells, adhesive bounding to a thermoplastic is required. In particular, formation of adhesive bonds to encapsulation layers is required to protect the active layers from environmental species, such as water[49].

CONCLUSION

To overcome challenges with bonding to polymers, this work presents ALD as a strategy for increasing the surface energy of polymers. For ALD Al_2O_3 on PMMA and FEP, VPI interphases were observed underneath the dense ALD Al_2O_3 surface films by cross-sectional TEM. The ALD Al_2O_3 film increased the surface energy of PMMA from 34.5±1.0 mJ m^{-2} to 844±63 mJ m^{-2} and the surface energy of FEP from 21.9±1.1 mJ m^{-2} to 955±224 mJ m^{-2}. After ALD film growth, the interfacial toughness of the PMMA-epoxy and FEP-epoxy interfaces in dry environments increased by a factor of 7 and 60, respectively. These results demonstrate that ALD can modify the surface chemistry of relatively inert substrates such as polymers to improve wettability, adhesion, and interfacial toughness, without affecting their bulk mechanical response or surface roughness. However, the interfacial toughness of the ALD-treated interfaces in the present system showed a strong dependence on humidity. It is clear that the use of a metal

oxides for these applications may cause significant sensitivity to ambient humidity, and this phenomenon of stress-corrosion cracking must be considered when designing such tailored interfaces.

ASSOCIATED CONTENT

Supporting Information.

The following files are available free of charge.

Experimental details; contact angle measurements; optical microscopy analysis; bulk mechanical testing of polymers; (PDF)

ACKNOWLEDGMENT

This work was supported by the Air Force Office of Scientific Research (AFOSR) under Grant FA9550-16-1-0313. This material is based upon work supported by the National Science Foundation under grant No. 1751590. This material is based upon work supported by a National Science Foundation Graduate Research Fellowship under Grant DGE 1256260. The authors thank Dr. Jared Tracy for insightful discussions and Nicholas Wurtz for design of the wedge testing apparatus. The authors acknowledge the financial support of the University of Michigan College of Engineering and NSF grant #DMR-9871177, and technical support from the Michigan Center for Materials Characterization

ABBREVIATIONS

ALD, atomic layer deposition; PMMA, poly(methyl methacrylate); FEP, fluorinated ethylene propylene; PDMS, polydimethylsiloxane; VPI, vapor phase infiltration; TMA, trimethylaluminum; RH, relative humidity

REFERENCES

(1) Fan, X.; Chung, J. Y.; Lim, Y. X.; Li, Z.; Loh, X. J. Review of Adaptive Programmable Materials and Their Bioapplications. *ACS Appl. Mater. Interfaces* **2016**, *8* (49), 33351–33370. https://doi.org/10.1021/acsami.6b09110.

(2) McCoul, D.; Hu, W.; Gao, M.; Mehta, V.; Pei, Q. Recent Advances in Stretchable and Transparent Electronic Materials. *Adv. Electron. Mater.* **2016**, *2* (5), 1–51. https://doi.org/10.1002/aelm.201500407.

(3) Deng, S.; Djukic, L.; Paton, R.; Ye, L. Thermoplastic-Epoxy Interactions and Their Potential Applications in Joining Composite Structures - A Review. *Composites Part A: Applied Science and Manufacturing*. January 2015, pp 121–132. https://doi.org/10.1016/j.compositesa.2014.09.027.

(4) Molitor, P.; Barron, V.; Young, T. Surface Treatment of Titanium for Adhesive Bonding to Polymer Composites: A Review. *Int. J. Adhes. Adhes.* **2001**, *21* (2), 129–136. https://doi.org/10.1016/S0143-7496(00)00044-0.

(5) Owens, D. K.; Wendt, R. C. Estimation of the Surface Free Energy of Polymers. *J. Appl. Polym. Sci.* **1969**, *13* (8), 1741–1747. https://doi.org/10.1002/app.1969.070130815.

(6) Morris, C. E. Strong, Durable Adhesive Bonding: Some Aspects of Surface Preparation, Joint Design and Adhesive Selection. *Mater. Forum* **1993**, *17*, 211–218.

(7) Murphy, M. P.; Kim, S.; Sitti, M. Enhanced Adhesion by Gecko-Inspired Hierarchical Fibrillar Adhesives. *ACS Appl. Mater. Interfaces* **2009**, *1* (4), 849–855. https://doi.org/10.1021/am8002439.

(8) Kuddannaya, S.; Chuah, Y. J.; Lee, M. H. A.; Menon, N. V; Kang, Y.; Zhang, Y. Surface Chemical Modification of Poly(Dimethylsiloxane) for the Enhanced Adhesion and Proliferation of Mesenchymal Stem Cells. *ACS Appl. Mater. Interfaces* **2013**, *5* (19), 9777–9784. https://doi.org/10.1021/am402903e.

(9) Wingfield, J. R. J. Treatment of Composite Surfaces for Adhesive Bonding. *Int. J. Adhes. Adhes.* **1993**, *13* (3), 151–156. https://doi.org/10.1016/0143-7496(93)90036-9.

(10) Garcia, A.; Berthelot, T.; Viel, P.; Polesel-Maris, J.; Palacin, S. Microscopic Study of a Ligand Induced Electroless Plating Process onto Polymers. *ACS Appl. Mater. Interfaces* **2010**, *2* (11), 3043–3051. https://doi.org/10.1021/am100907j.

(11) Thakur, V. K.; Vennerberg, D.; Kessler, M. R. Green Aqueous Surface Modification of Polypropylene for Novel Polymer Nanocomposites. *ACS Appl. Mater. Interfaces* **2014**, *6* (12), 9349–9356. https://doi.org/10.1021/am501726d.

(12) Inagaki, N.; Tasaka, S.; Masumoto, M. Improved Adhesion between Kapton Film and Copper Metal by Plasma Graft Polymerization of Vinylimidazole. *Macromolecules* **1996**, *29* (5), 1642–1648. https://doi.org/10.1021/ma9503571.

(13) Mahlberg, R.; Niemi, H. E.-M.; Denes, F. S.; Rowell, R. M. Application of AFM on the Adhesion Studies of Oxygen-Plasma-Treated Polypropylene and Lignocellulosics. *Langmuir* **1999**, *15* (8), 2985–2992. https://doi.org/10.1021/la980139b.

(14) Schulz, U.; Munzert, P.; Kaiser, N. Surface Modification of PMMA by DC Glow Discharge and Microwave Plasma Treatment for the Improvement of Coating Adhesion. *Surf. Coatings Technol.* **2001**, *142–144*, 507–511. https://doi.org/10.1016/S0257-8972(01)01202-6.

(15) Hook, T. J.; Gardella, J. A.; Salvati, L. Multitechnique Surface Spectroscopic Studies of Plasma-Modified Polymers I: H2O/Ar Plasma-Modified Polymethylmethacrylates. *J. Mater. Res.* **1986**, *2* (01), 117–131. https://doi.org/10.1557/jmr.1987.0117.

(16) Sheng, E.; Sutherland, I.; Brewis, D. M.; Heath, R. J.; Bradley, R. H. Surface Studies of Polyethylene Modified by Flame Treatment. *J. Mater. Chem.* **1994**, *4* (3), 487–490. https://doi.org/10.1039/jm9940400487.

(17) Roy, A. K.; Dendooven, J.; Deduytsche, D.; Devloo-Casier, K.; Ragaert, K.; Cardon, L.; Detavernier, C. Plasma-Enhanced Atomic Layer Deposition: A Gas-Phase Route to Hydrophilic, Glueable Polytetrafluoroethylene. *Chem. Commun.* **2015**, *51* (17), 3556–3558. https://doi.org/10.1039/c4cc09474c.

(18) Kääriäinen, T. O.; Cameron, D. C.; Tanttari, M. Adhesion of Ti and TiC Coatings on PMMA Subject to Plasma Treatment: Effect of Intermediate Layers of Al2O3 and TiO2 Deposited by Atomic Layer Deposition. *Plasma Process. Polym.* **2009**, *6* (10), 631–641. https://doi.org/10.1002/ppap.200900038.

(19) Hyde, G. K.; Scarel, G.; Spagnola, J. C.; Peng, Q.; Lee, K.; Gong, B.; Roberts, K. G.; Roth, K. M.; Hanson, C. A.; Devine, C. K.; Stewart, S. M.; Hojo, D.; Na, J. S.; Jur, J. S.; Parsons, G. N. Atomic Layer Deposition and Abrupt Wetting Transitions on Nonwoven Polypropylene and Woven Cotton Fabrics. *Langmuir* **2010**, *26* (4), 2550–2558. https://doi.org/10.1021/la902830d.

(20) Ferguson, J. D.; Weimer, A. W.; George, S. M. Atomic Layer Deposition of Al2O3 Films on Polyethylene Particles. *Chem. Mater.* **2004**, *16* (26), 5602–5609. https://doi.org/10.1021/cm040008y.

(21) Elam, J. W.; Routkevitch, D.; Mardilovich, P. P.; George, S. M. Conformal Coating on Ultrahigh-Aspect-Ratio Nanopores of Anodic Alumina by Atomic Layer Deposition. *Chem. Mater.* **2003**, *15* (18), 3507–3517. https://doi.org/10.1021/cm0303080.

(22) Groner, M. D.; Fabreguette, F. H.; Elam, J. W.; George, S. M. Low-Temperature Al2O3 Atomic Layer Deposition. *Chem. Mater.* **2004**, *16* (4), 639–645. https://doi.org/10.1021/cm0304546.

(23) Leng, C. Z.; Losego, M. D. Vapor Phase Infiltration (VPI) for Transforming Polymers into Organic–Inorganic Hybrid Materials: A Critical Review of Current Progress and Future Challenges. *Mater. Horiz.* **2017**, *4* (5), 747–771. https://doi.org/10.1039/C7MH00196G.

(24) Parsons, G. N.; Atanasov, S. E.; Dandley, E. C.; Devine, C. K.; Gong, B.; Jur, J. S.; Lee, K.; Oldham, C. J.; Peng, Q.; Spagnola, J. C.; Williams, P. S. Mechanisms and Reactions during Atomic Layer Deposition on Polymers. *Coordination Chemistry Reviews*. 2013, pp

3323–3331. https://doi.org/10.1016/j.ccr.2013.07.001.

(25) Peng, Q.; Tseng, Y.-C.; Long, Y.; Mane, A. U.; Didona, S.; Darling, S. B.; Elam, J. W. Effect of Nanostructured Domains in Self-Assembled Block Copolymer Films on Sequential Infiltration Synthesis. *Langmuir* **2017**, *33*, 13214–13223. https://doi.org/10.1021/acs.langmuir.7b02922.

(26) Peng, Q.; Tseng, Y. C.; Darling, S. B.; Elam, J. W. Nanoscopic Patterned Materials with Tunable Dimensions via Atomic Layer Deposition on Block Copolymers. *Adv. Mater.* **2010**, *22* (45), 5129–5133. https://doi.org/10.1002/adma.201002465.

(27) Wilson, C. A.; Grubbs, R. K.; George, S. M. Nucleation and Growth during Al 2O 3 Atomic Layer Deposition on Polymers. *Chem. Mater.* **2005**, *17* (23), 5625–5634. https://doi.org/10.1021/cm050704d.

(28) Jur, J. S.; Spagnola, J. C.; Lee, K.; Gong, B.; Peng, Q.; Parsons, G. N. Temperature-Dependent Subsurface Growth during Atomic Layer Deposition on Polypropylene and Cellulose Fibers. *Langmuir* **2010**, *26* (11), 8239–8244. https://doi.org/10.1021/la904604z.

(29) Akyildiz, H. I.; Padbury, R. P.; Parsons, G. N.; Jur, J. S. Temperature and Exposure Dependence of Hybrid Organic− Inorganic Layer Formation by Sequential Vapor Infiltration into Polymer Fibers. **2012**, *28*, 15697–15704. https://doi.org/10.1021/la302991c.

(30) Oss, C. J. van; Chaudhury, M. K.; Good, R. J. Interfacial Lifshitz-van Der Waals and Polar Interactions in Macroscopic Systems. *Chem. Rev.* **1988**, *88* (6), 927–941. https://doi.org/10.1021/cr00088a006.

(31) Preston, D. J.; Song, Y.; Lu, Z.; Antao, D. S.; Wang, E. N. Design of Lubricant Infused Surfaces. *ACS Appl. Mater. Interfaces* **2017**, *9* (48), 42383–42392. https://doi.org/10.1021/acsami.7b14311.

(32) Thouless, M. D. Shear Forces, Root Rotations, Phase Angles and Delamination of Layered Materials. *Eng. Fract. Mech.* **2018**, *191*, 153–167. https://doi.org/10.1016/j.engfracmech.2018.01.033.

(33) Padbury, R. P.; Jur, J. S. Effect of Polymer Microstructure on the Nucleation Behavior of Alumina via Atomic Layer Deposition. *J. Phys. Chem. C* **2014**, *118* (32), 18805–18813. https://doi.org/10.1021/jp506456y.

(34) Gong, B.; Parsons, G. N. Quantitative in Situ Infrared Analysis of Reactions between Trimethylaluminum and Polymers during Al 2O 3 Atomic Layer Deposition. *J. Mater. Chem.* **2012**, *22* (31), 15672–15682. https://doi.org/10.1039/c2jm32343e.

(35) Xu, Q.; Yang, Y.; Wang, X.; Wang, Z.; Jin, W.; Huang, J.; Wang, Y. Atomic Layer Deposition of Alumina on Porous Polytetrafluoroethylene Membranes for Enhanced Hydrophilicity and Separation Performances. *J. Memb. Sci.* **2012**, *415–416*, 435–443. https://doi.org/10.1016/j.memsci.2012.05.031.

(36) Biswas, M.; Libera, J. A.; Darling, S. B.; Elam, J. W. New Insight into the Mechanism of

Sequential Infiltration Synthesis from Infrared Spectroscopy. *Chem. Mater.* **2014**, *26* (21), 6135–6141. https://doi.org/10.1021/cm502427q.

(37) Biswas, M.; Libera, J. A.; Darling, S. B.; Elam, J. W. Kinetics for the Sequential Infiltration Synthesis of Alumina in Poly(Methyl Methacrylate): An Infrared Spectroscopic Study. *J. Phys. Chem. C* **2015**, *119* (26), 14585–14592. https://doi.org/10.1021/jp511939j.

(38) Dandley, E. C.; Needham, C. D.; Williams, P. S.; Brozena, A. H.; Oldham, C. J.; Parsons, G. N. Temperature-Dependent Reaction between Trimethylaluminum and Poly(Methyl Methacrylate) during Sequential Vapor Infiltration: Experimental and Ab Initio Analysis. *J. Mater. Chem. C* **2014**, *2* (44), 9416–9424. https://doi.org/10.1039/C4TC01293C.

(39) Kemell, M.; Färm, E.; Ritala, M.; Leskelä, M. Surface Modification of Thermoplastics by Atomic Layer Deposition of Al2O3 and TiO2 Thin Films. *Eur. Polym. J.* **2008**, *44* (11), 3564–3570. https://doi.org/10.1016/j.eurpolymj.2008.09.005.

(40) Dann, J. R. Forces Involved in the Adhesive Process. I. Critical Surface Tensions of Polymeric Solids as Determined with Polar Liquids. *J. Colloid Interface Sci.* **1970**, *32* (2), 302–320. https://doi.org/10.1016/0021-9797(70)90054-8.

(41) Ebnesajjad, S.; Ebnesajjad, C. *Surface Treatment of Materials for Adhesion Bonding*; William Andrew Publishing, 2006.

(42) Jeurgens, L.; Sloof, W.; Tichelaar, F.; Mittemeijer, E. Thermodynamic Stability of Amorphous Oxide Films on Metals: Application to Aluminum Oxide Films on Aluminum Substrates. *Phys. Rev. B - Condens. Matter Mater. Phys.* **2000**, *62* (7), 4707–4719. https://doi.org/10.1103/PhysRevB.62.4707.

(43) Kinloch, A. J. *Adhesion and Adhesives*; 1987. https://doi.org/10.1007/978-94-015-7764-9.

(44) Shen, J.; Chen, C. C.; Sauer, J. A. Effects of Sorbed Water on Properties of Low and High Molecular Weight PMMA: 1. Deformation and Fracture Behaviour. *Polymer (Guildf).* **1985**, *26* (4), 511–518. https://doi.org/10.1016/0032-3861(85)90150-8.

(45) Beaumont, P. W. R.; Young, R. J. *Failure of Brittle Polymers by Slow Crack Growth - Part 1 Crack Propagation in Polymethylmethacrylate and Time-to-Failure Predictions*; 1975; Vol. 10. https://doi.org/10.1007/BF00540823.

(46) Sacher, E.; Susko, J. R. Water Permeation of Polymer Films. II. Dual-Mode Absorption in Teflon FEP. *J. Appl. Polym. Sci.* **1979**, *24* (9), 1997–2003.

(47) De Aza, A. H.; Chevalier, J.; Fantozzi, G.; Schehl, M.; Torrecillas, R. Crack Growth Resistance of Alumina, Zirconia and Zirconia Toughened Alumina Ceramics for Joint Prostheses. *Biomaterials* **2002**, *23* (3), 937–945. https://doi.org/10.1016/S0142-9612(01)00206-X.

(48) Ebrahimi, M. E.; Chevalier, J.; Fantozzi, G. Slow Crack-Growth Behavior of Alumina Ceramics. *J. Mater. Res.* **2000**, *15* (1), 142–147. https://doi.org/10.1557/JMR.2000.0024.

(49) Kim, N.; Potscavage, W. J.; Domercq, B.; Kippelen, B.; Graham, S. A Hybrid Encapsulation Method for Organic Electronics. *Appl. Phys. Lett.* **2009**, *94* (16).

https://doi.org/10.1063/1.3115144.

Table of Contents Graphic